ORIGINAL PAPER

Synthesis and luminescence investigation of $Ba_2V_2O_7$-co-doped Dy^{3+}/ Eu^{3+} phosphors for white light-emitting diode applications

N Venkatesh Bharathi[1,2], P Kavitha[2], S Ramaswamy[1,2]*, S S Jayabalakrishnan[2] and K Sakthipandi[3]* (ORCID)

[1]P.G. and Research Department of Physics, N.M.S.S.V.N. College, Madurai, Tamil Nadu 625 019, India

[2]Department of Physics, Mannar Thirumalai Naicker College, Pasumalai, Madurai, Tamil Nadu 625004, India

[3]Department of Physics, SRM TRP Engineering College, Tiruchirappalli, Tamil Nadu 621 105, India

Abstract: This study is aimed to tune the $Ba_2V_2O_7$ phosphors as the potential candidates in the fabrication of ultra-violet (UV) or near-UV chip-excited white light-emitting diodes (WLEDs) by incorporating Dy^{3+} and Eu^{3+} ions in the host lattice. A series of Dy^{3+} and Eu^{3+} ions-doped $Ba_2V_2O_7$ phosphor materials was synthesized using the hydrothermal method. Phase purity, structural, optical, and luminescence characteristics of as-synthesized Dy^{3+} and Eu^{3+} ions-doped $Ba_2V_2O_7$ phosphors were studied using powder X-ray diffraction (XRD), UV–visible spectroscopy, and fluorescence spectrometry. The XRD patterns of Dy^{3+} and Eu^{3+} ions-doped $Ba_2V_2O_7$ phosphors were indexed with triclinic structure as parent $Ba_2V_2O_7$ phosphor compounds. The broad absorption in the UV region was originated from the parent $Ba_2V_2O_7$ phosphors ($[VO_4]^{3-}$) group charge transfer (CT). The overall emission peak centered at 495 nm was due to the charge transfer band (CTB) of the $[VO_4]^{3-}$ group. In addition, the sharp peaks observed in the visible to near-infrared (NIR) region also originated due to CT from the dopant Dy^{3+}/Eu^{3+} ions. The charge transition of Dy^{3+} and Eu^{3+} ions with the parent leads to sharp peaks, observed from 570 to 710 nm. The photoluminescence (PL) spectra recorded at 348 nm emission color tuned from bluish-white to greenish-yellow. The irradiation observed the white color emission of Dy^{3+} and Eu^{3+} ions-doped $Ba_2V_2O_7$ phosphors under the UV light 365 nm. Hence, the results have suggested that the as-prepared Dy^{3+} and Eu^{3+} ions-doped $Ba_2V_2O_7$ phosphors are the potential candidates for fabricating a UV or near-UV chip-excited WLEDs.

Keywords: Hydrothermal method; Structural properties, luminescence; Charge transfer transition; WLEDs

1. Introduction

In recent years, considerable interest has been paid to the 4f state and the trivalent Lanthanide (Ln^{3+})-doped inorganic phosphor materials, which exhibit fascinating luminescent properties [1] due to the Ln^{3+} states intraelectronic transition. Ln^{3+}-doped luminescent materials are primarily applied in conventional/traditional information display technologies, novel, emerging lighting, biomedical technologies, and other applications [2–5]. These luminescent materials exhibit excellent energy conversion efficiency, strong emission bands, long-lived excited electronic states, good thermal conductivity, and stability [6, 7].

The next generation of solid-state lighting for the white light-emitting diode (WLED) attracts a lot of research attention and a wide range of applications due to their extended practical lifetime, compactness, high durability, and being environmentally friendly [8–10]. Generally, three primary methods were used for WLED fabrication: (i) multichip LED, which uses a tricolor mixing phosphor to achieve complete absorption in the visible region, and (ii) phosphor conversion LED, which uses UV light activation to achieve white light, and (iii) the blue LED combined with a yellow phosphor which stimulates white spectrum [11–13]. The commercial WLED was fabricated by the third method by combining the blue-emitting chip with $Y_3Al_5O_{12}:Ce^{3+}$ yellow-emitting phosphor. These WLEDs have a drawback of the poor color rendering index (CRI) due to low red emission in the visible spectrum [14–16]. Therefore, many efforts have been made to

*Corresponding author, E-mail: ramaswamysvn@gmail.com; sakthipandi@gmail.com

overcome drawbacks to preparing the efficient and chemically stable phosphor material.

Inorganic vanadate phosphors offer applications because of their broad and intense CT band in the near-ultraviolet (NUV) and ultraviolet (UV) regions. Usually, luminescent materials based on vanadate emit distinct wavelengths across a wide range of visible wavelengths [17]. In past decades, Ln^{3+}-activated inorganic vanadates host phosphor which have a considerable attention in flat panel display, white light, and fluorescent lamps [18–20], etc. So far, plenty of Ln^{3+}-doped and co-doped vanadate host materials is reported as a prospective phosphor in the generation of WLED applications. These types of phosphors contain red, green, and blue (RGB) emissions within the same host matrix because they can powerfully absorb the UV light and subsequently transfer the energy to Ln^{3+}-ions [21–24].

A self-activated $Ba_2V_2O_7$ phosphor with excellent luminescent material for UV chip-excited WLED application was recently described in our earlier studies [25]. This material had the disadvantage of low red emission in the visible region. To address this shortcoming, researchers attempted to produce the most efficient single phased Ln^{3+} ions-co-doped vanadate-based white-light-emitting phosphors. Usually, Ln^{3+} activators such as europium (Eu^{3+}) and dysprosium (Dy^{3+}) ions were previously known for their strong emission in the visible region under the excitation of NUV or UV lights [26–29].

Eu^{3+}-doped vanadates were excellent luminescent materials with strong red emissions attributed to the $^5D_0 \rightarrow {}^7F_J$ (J = 1, 2, 3, 4) transitions [30–32]. Similarly, the Dy^{3+} ion exhibits three dominant emissions in the blue ($^4F_{9/2} \rightarrow {}^6H_{15/2}$), yellow ($^4F_{9/2} \rightarrow {}^6H_{13/2}$), and red ($^4F_{9/2} \rightarrow {}^6H_{11/2}$) emissions [33–35]. The emission color tuning can generally be obtained from Dy^{3+}/Eu^{3+}-co-doped vanadate materials, which arose abundant CT from VO_4^{3-} group $\rightarrow Dy^{3+} \rightarrow Eu^{3+}$ ions. Therefore, Dy^{3+}/Eu^{3+} ions-co-doped vanadate phosphors in solid-state lighting applications have received much attention.

Only a few studies have focused on the Dy^{3+-}/Eu^{3+}-co-doped vanadates host phosphor until now. Yuexin Wang et al. [36] used a solvothermal approach to create a series of color tunable $LuVO_4$:Tm^{3+}, Dy^{3+}, and Eu^{3+} phosphors. They have analytically studied the luminescent properties of the co-doped and tri-doped activators for solid-state lighting applications in a systematic manner. The dopant and excitation wavelength of color tunability of Dy^{3+}:YVO_4 and Dy^{3+}/Eu^{3+}:YVO_4 phosphors were explored by Anna M. Kaczmarek et al. [37]. Due to the appropriate doping concentration, these phosphors were prepared by the hydrothermal method and obtained white light emission. Xuemei Zhang et al. [38] used a one-step green hydrothermal approach to successfully synthesize the multi-color emitting $ScVO_4$:Ln^{3+} ($Ln^{3+} = Eu^{3+}$, Dy^{3+}, Eu^{3+}/Dy^{3+}) microcrystal phosphor.

They were able to change the color of the emission from blue and yellow to red by altering the concentration of the activators. For multifunctional applications, it used a variety of excitation wavelengths at consistent doping concentrations. Xiulan Wu et al. [39] prepared a single phased white light-emitting KBa(VO_4): Dy^{3+}/ Eu^{3+} phosphors by the solid-state reaction method. The color of the emission was adjusted by altering the doping concentration. This study describes Dy^{3+-}/Eu^{3+}-co-doped $Ba_2V_2O_7$ phosphors by a simple and effective hydrothermal method. The nature of the crystal, optical properties, luminescent properties, energy transfer efficiency, and colorific properties are investigated in detail.

2. Experimental details

LOBA chemicals, India, provided high purity (99%) Barium nitrate ($Ba(NO_3)_2$), dysprosium oxide (Dy_2O_3), ammonia solution (NH_4), europium oxide (Eu_2O_3), and sodium metavanadate ($NaVO_3$). These were of analytical grade chemicals and were used without any further purification. Distilled water was used as the solvent throughout the synthesis protocol. $Ba_2V_2O_7$:0.04-Dy^{3+},xEu^{3+} phosphors (x = 0.01, 0.02, 0.03, 0.04 & 0.05) were prepared by the hydrothermal method [25]. 8.15 g of $Ba(NO_3)_2$ and 1.95 g $NaVO_3$ were dissolved separately in 40 ml of distilled water. The combined solution was stirred for 15 min. 0.12 g of Dy_2O_3 was dissolved in 2 ml nitric acid and mildly heated to obtain dysprosium nitrate. Similarly, 0.028 g of Eu_2O_3 was dissolved into 2 ml nitric acid and mildly heated to obtain europium nitrate. These dysprosium nitrate and europium nitrate mixtures were added to the source material under vigorous stirring. The pH level of the stirred solution was adjusted to about 12 using the ammonia solution with continuous stirring. After adjusting pH, the solution was stirred for one hour. The mixed solution was transferred in a Teflon-lined autoclave with a capacity of 100 ml and tightly sealed. The solution in the autoclave was heated to 180 °C for 48 h in a muffle furnace, which was then cooled to room temperature naturally. The precipitate was filtered and washed several times with distilled water. The final white color powder was obtained after a few hours of drying at 60 °C on a hot plate. $Ba_{2-x}Dy_{0.04}Eu_xV_2O_7$ phosphor was synthesized and termed as BD04E01, BD04E02, BD04E03, BD04E04, and BD04E05, respectively, for the composition x = 0.01, 0.02, 0.03, 0.04, and 0.05.

A PANalytical XPERT-PRO Diffractometer, Japan, with Cu-K radiation was used to conduct X-ray diffraction experiments on the produced powder in the scan range of

10°–60°. The diffused reflectance spectra (DRS) were measured using a UV-2600 SHIMADZU spectrophotometer, Japan, using BaSO$_4$ as a non-absorbing standard reference from 200 to 1200 nm. A Shimadzu RF-5301PC Spectrofluorometer, Japan, was used to record photoluminescence (PL) spectra. The chromaticity color coordinates of the Commission International de l'Eclairage (CIE) were determined using the GOCIE Version 2 CIE-1931 plot program. At room temperature, all of the experiments were carried out.

3. Results and discussion

3.1. Structural analysis

Powder XRD patterns of as-prepared BD04E01, BD04E02, BD04E03, BD04E04, and BD04E05 phosphors are shown in Fig. 1. All the diffraction patterns were indexed to the triclinic phase of Ba$_2$V$_2$O$_7$ in JCPDS card 76–0612. The position of the prominent diffracted peak was slightly shifted to a higher angle when the doping concentration of Eu^{3+} added up. Such peak shift was related to the lattice expansion after doping. This was due to the ion radii of Dy^{3+} (r = 0.108 nm) and Eu^{3+} (r = 0.095 nm) which was smaller than Ba^{2+} (r = 0.14 nm) ion radius [40, 41]. This observation obeys Vegard's law [42]. XRD result shows that Dy^{3+} and Eu^{3+} ions have been successfully incorporated into the Ba^{2+} lattice site in the Ba$_2$V$_2$O$_7$ host without any structural change. Further, the increase in the relative XRD intensity of (102) diffraction peak was observed due to the ordered crystallization arrangement. The doping concentration was minimal. Therefore, the increase in Eu^{3+} doping concentration leads to an increase in the crystalline nature of the samples. The acceptable percentage difference (D_r) between the radius of substituted Ba^{2+} ion (R_s)

and the radius of dopant Eu^{3+} ion (R_d) should not be more than 30% which was obtained by the formula [43]:

$$D_r = \frac{R_s - R_d}{R_s} \times 100\% \tag{1}$$

In the present case, the estimated value of D_r for the as-prepared phosphors was found to be 28%, which is less than 30%. Therefore, it was successfully confirmed that incorporating the Eu^{3+} ion into the Ba^{2+} lattice site in the Ba$_2$V$_2$O$_7$ host was done without any structural change.

3.2. UV–Visible–NIR spectral analysis

Figure 2a shows the diffused reflectance spectra of the as-synthesized BD04E01, BD04E02, BD04E03, BD04E04, and BD04E05 phosphors in the range of 200–1200 nm. The band observed at 215 nm was due to the transition of O^{2-} → Dy^{3+}/Eu^{3+}. The broadband in the range of 250–340 nm centered at 300 nm was due to the charge transfer band of O^{2-} → V^{5+} [44]. The sharp peaks observed from the visible to NIR region (400–1200 nm)
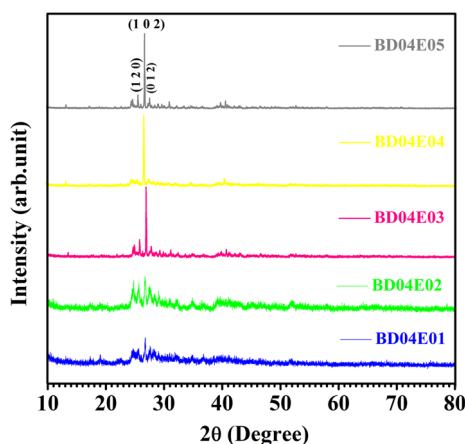

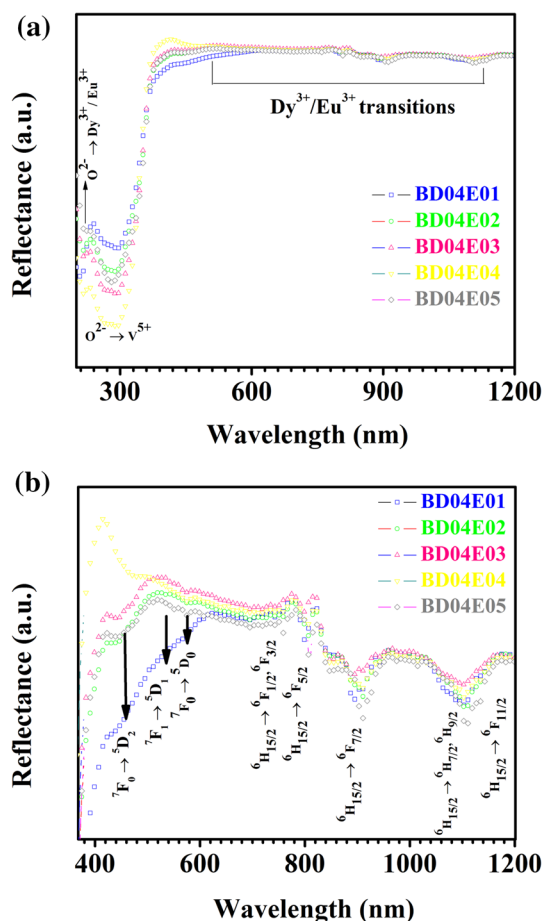**Fig. 2** (**a**) Diffuse reflectance spectra and (**b**) the enlarged view of peaks in the range 400–1200 nm of BD04E01, BD04E02, BD04E03, BD04E04, and BD04E05 phosphors

Fig. 1 Powder XRD patterns of BD04E01, BD04E02, BD04E03, BD04E04, and BD04E05 phosphors

were due to the intra 4f CT of Ln^{3+} [45]. Figure 2b depicts the diffused reflectance spectra of the as-prepared BD04E01, BD04E02, BD04E03, BD04E04, and BD04E05 phosphors in the range of 400–1200 nm. Several absorption peaks were observed at 758, 807, 908, 975, 1103, and 1184 nm. They were corresponding to the intra 4f CT of the Dy^{3+} ions, and the peaks at 468, 539, and 574 nm corresponded to the intra 4f CT of the Eu^{3+} ions.

These peaks were assigned to the CT from the ground state $^6H_{15/2}$ to various excited states $^6F_{1/2}$, $^6F_{3/2}$, $^6F_{5/2}$, $^6F_{7/2}$, $^6F_{9/2}$, $^6F_{11/2}$ of the Dy^{3+} ions, and $^7F_0$, $^7F_1$ to $^5D_2$, $^5D_1$, $^5D_0$ states of the Eu^{3+} ions, respectively [46–48]. This result confirmed that the formation of a meta-stable state between the valence and the conduction band is due to the substitution of the Eu^{3+} ions in all as-prepared BD04E01, BD04E02, BD04E03, BD04E04, and BD04E05 phosphor. Further, using diffuse reflectance spectra the band gap of the BD04E01, BD04E02, BD04E03, BD04E04, and BD04E05 phosphors can be achieved using the Kubelka–Munk theory. In the DR spectra, the ratio of the light scattered from a thick layer of the sample and an ideal non-absorbing reference sample is measured as a function of the wavelength λ, $R = R_{sample}/R_{reference}$. The relationship between the diffuse reflectance of the sample (R), the absorption coefficient (K), and the scattering coefficient (S) is given by the Kubelka–Munk function F(R):

$$F(R) = \frac{K}{S} = \frac{(1-R)^2}{2R} \tag{2}$$

where K, S, and R represent the absorption coefficient, scattering coefficient, and observed reflectivity, respectively.

The linear absorption coefficient α and the optical band gap (E_g) of the as-prepared BD04E01, BD04E02, BD04E03, BD04E04, and BD04E05 phosphors can be related by the Tauc relation expressed as Eq. (3):

$$(\alpha h\gamma)^2 = A(h\gamma - E_g)^n \tag{3}$$

where A is proportionality constant, $h\upsilon$ is the photon energy, and E_g is the band-gap energy. When the material scatters in a perfectly diffuse manner, the absorption coefficient K becomes equal to 2α. Considering the scattering coefficient S, a constant with respect to the wavelength, and using above two equations, the following expression can be written as:

$$(F(R_\infty)h\gamma)^2 = B(h\gamma - E_g)^n \tag{4}$$

The value of n is ½ for direct type transition and 2 for an indirect type transition.

The estimated band gap values of the as-synthesized phosphors are shown in Fig. 3. The estimated values of the band-gap energy for BD04E01, BD04E02, BD04E03,
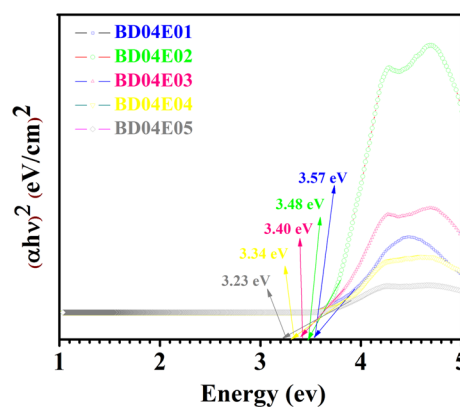

Fig. 3 Tauc plot for determining the band gap of BD04E01, BD04E02, BD04E03, BD04E04, and BD04E05 phosphors

BD04E04, and BD04E05 phosphors were 3.57, 3.48, 3.40, 3.34, and 3.23 eV, respectively. The reason behind the lowering of band gap with the addition of Eu^{3+} ion is the formation of meta-stable state between the valence band and the conduction band (i.e., in between direct band-gap) [49]. Similar band-gap difference was observed for $Y_{1-x}Gd_xVO_4$:0–0.2% Dy^{3+} ($x = 0$, 0.25, 0.50, 0.75 and 1.00) phosphor by Puja Kumari and J. Manam [50].

3.3. Photoluminescence spectral analysis

The excitation spectra of the as-prepared BD04E01, BD04E02, BD04E03, BD04E04, and BD04E05 phosphors were monitored under the red emission (613 nm) wavelength shown in Fig. 4. The intense broad band peak at 348 nm in the excitation spectra was attributed to the $O^{2-} \rightarrow V^{5+}$ bond CT in the host matrix. When the concentration of Eu^{3+} increased, the sharp peak appeared at 305 nm for $x = 0.04$ was due to the second harmonic generation [51–53]. The strong signal peak at 305 nm for BD04E04 and BD04E05 phosphors was owing to the CT from O^{2-} to Dy^{3+}/Eu^{3+}. Ion Eu^{3+} inner 4f-shell excitation
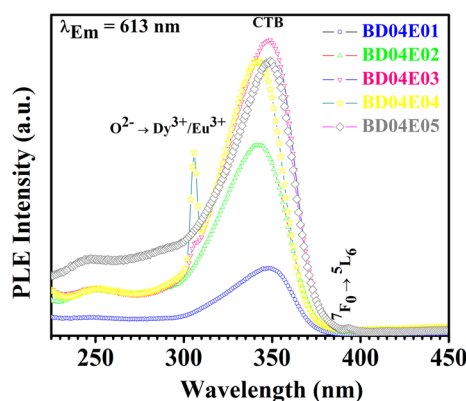

Fig. 4 PLE spectra of BD04E01, BD04E02, BD04E03, BD04E04, and BD04E05 phosphors monitored at 613 nm emission

caused the 393 nm peak [54]. This indication means that near-UV light, like CTB, could ignite these phosphors used in solid-state lighting.

Upon the 348 nm excitation, the PL emission spectra of the as-synthesized phosphors were monitored in the range from 400 to 800 nm and are shown in Fig. 5. The PL emission spectra consist of the broad emission in the range 400 to 565 nm due to the localized charge transfer from V^{5+} to O^{2-} in the VO$_4$ group. The sharp emission peaks exhibited at 572, 613, and 687 nm were owing to the co-dopant Dy^{3+}/Eu^{3+} ions in the Ba$_2$V$_2$O$_7$ host. The yellow emission peak at 572 nm was linked to the transition ^{4}F$_{9/2} \rightarrow {}^6$H$_{13/2}$ of the Dy^{3+} ion [55, 56]. The orange-red emission peak at 613 nm was matched to the hypersensitive transition ^{5}D$_0 \rightarrow {}^7$F$_2$ of the Eu^{3+} ion. This transition intensity was highly impacted by the local symmetry of the Eu^{3+} ion and the composition of the ligands than the intensities of the other induced electric dipole transitions.

Due to the Eu^{3+} ion, a red emission peak appeared at 687 nm corresponding to the transition ^{5}D$_0 \rightarrow {}^7$F$_4$. This transition has excellent intensity, followed by ^{5}D$_0 \rightarrow {}^7$F$_2$. The intensity of the hypersensitive transitions ^{5}D$_0 \rightarrow {}^7$F$_2$, and ^{7}F$_4$ was altered dramatically with the chemical environment [57–59]. While the doping concentration of the Eu^{3+} increased, the overall, emission peak intensity was found to increase maximum in BD04E03 phosphors. With further increased concentration, the peak intensity was decreased for BD04E04 and BD04E05 phosphors. The dopant transition peaks increased the maximum for BD04E01, BD04E02, BD04E03, and BD04E04 phosphors and further increased the doping concentration. The peak intensity was decreased in BD04E05 phosphors because of the concentration quenching effect [60]. The change in the position of the peak was under the excitation wavelength and strictly at a double wavelength. It clearly shows that it was a second harmonic generation. This result shows that
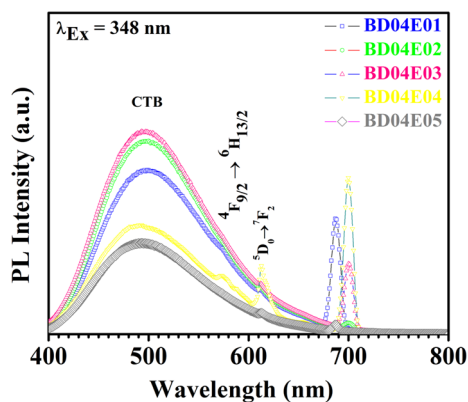
the luminescence property of the co-doped rare-earth ion depends on the excitation wavelength.

The critical distance (R_c) of BD04E01, BD04E02, BD04E03, BD04E04, and BD04E05 phosphors was examined based on the Blasse's theory [61]. For certain [VO$_4$]$^{3-}$ system, the R_c is defined as the distance for which the probability of energy transfer equals the probability of radiation emission of energy donator. The R_c between [VO$_4$]$^{3-}$ and Eu^{3+} was estimated from the following Eq. (5):

$$R_c \approx 2 \left[\frac{3V}{4\pi X_c N} \right]^{1/3} \tag{5}$$

where V is the volume of the unit cell, N is the number of host lattice cations in the unit cell, and X_c is the critical concentration of activator ion [Eu^{3+}]. From the above equation, the critical energy transfer distance was estimated and is shown in Table 1, which was more significant than the critical distance, $R_c = 5$ Å.

Dexter [62] reported two kinds of energy transfer mechanisms depending on the actual distance between the sensitizer and activator ions. They were exchanging inter-actions and multipolar interactions. If the value of the critical distance is about 3–4 Å, the exchange interaction may occur. If the value was more significant than 5 Å, the sensitizer and activator orbits overlap, and the multipolar interactions may dominate. The above observation concludes that the type of energy transfer mechanism between the sensitizer [VO$_4$]$^{3-}$ and the activator Eu^{3+} ion (Ba$_{2-x}$Dy$_{0.04}$Eu$_x$V$_2$O$_7$) phosphor system belongs to multipolar interactions. Dexture's reports revealed that the multipolar interaction occurs during the interaction between sensitizer and activator. This multipolar interaction will cause a non-radiative energy transfer. The following Eq. (6) determines it:

$$\frac{1}{x} = \frac{K}{1 + \beta x^{Q/3}} \tag{6}$$

where K & β are constants, x is the doping concentration of Eu^{3+} ions. The exchange interactions, such as dipole–

Fig. 5 PL spectra of BD04E01, BD04E02, BD04E03, BD04E04, and BD04E05 phosphors monitored at 348 nm

Table 1 Values of critical distance (R_c) and its energy transfer coefficient (Q) for the as-prepared BD04E01, BD04E02, BD04E03, BD04E04, and BD04E05 phosphors were listed

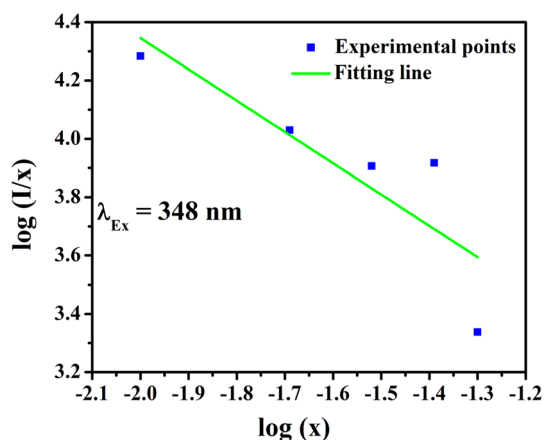| X_c in %	N	V in Å^3	R_c in Å	Q
0.01			20.15	
0.02			17.31	
0.03	8	377.841	15.25	3.09
0.04			13.15	
0.05			11.12	

Fig. 6 Dependence of log (I/x) on log (x) of BD04E01, BD04E02, BD04E03, BD04E04, and BD04E05 phosphors under 348 nm excitation

dipole, dipole–quadrupole, and quadrupole–quadrupole interactions, are represented by the value of Q = 3, 6, 8 & 10 [63]. The above equation can be rearranged as follows (Eq. (7)) if $\beta x^{Q/3} >> 1$ [64]:

$$\log\left(\frac{1}{x}\right) = A - \frac{Q}{3}\log x \tag{7}$$

where $A = \log K - \log \beta$. By using this equation, Fig. 6 ($\lambda_{Ex} = 348$ nm) is plotted for log ($1/x$) against log (x) for BD04E01, BD04E02, BD04E03, BD04E04, and BD04E05 phosphor. The slope of these curves for the emission spectra stimulated at 348 nm is determined from Fig. 6. The value is -1.76 nm, respectively, and corresponding Q value is shown in Table 1. It was approximately closer to Q = 3. This result shows that the concentration quenching mechanism of Eu^{3+} ion in $Ba_{2-x}Dy_{0.04}Eu_xV_2O_7$ phosphor host was due to exchange interaction.

3.4. Photometric studies

As-synthesized $Ba_{2-x}Dy_{0.04}Eu_xV_2O_7$ phosphor was excited/stimulated at 348 nm, and the corresponding chromaticity CIE diagram is shown in Fig. 7. The photographic images of the as-prepared BD04E01, BD04E02, BD04E03, BD04E04, and BD04E05 phosphors were taken in the daylight and irradiated under the UV light at 365 nm. In the daylight, BD04E01, BD04E02, BD04E03, BD04E04, and BD04E05 phosphors appeared to be white in color. The as-prepared phosphors irradiated under UV light at 365 nm turn glaring white to bluish-white color as the Eu^{3+} concentration increases, as shown in Fig. 8. The CIE chromaticity coordinates, CRI, and CCT values of the $Ba_{2-x}Dy_{0.04}Eu_xV_2O_7$ phosphors are tabulated in Table 1.

The CRI and CCT values were calculated from the PL emission spectra of the as-prepared $Ba_{2-x}Dy_{0.04}Eu_xV_2O_7$
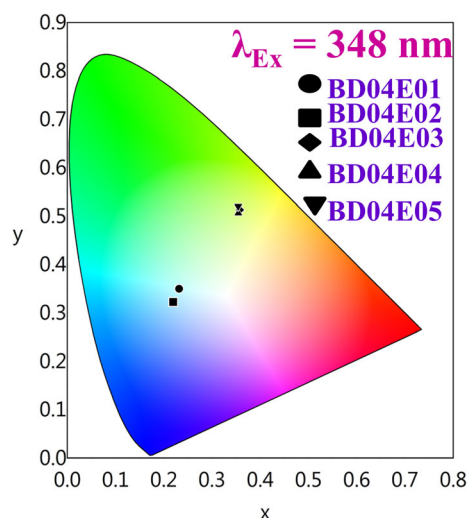

Fig. 7 CIE chromaticity diagram showing the emission colors of BD04E01, BD04E02, BD04E03, BD04E04, and BD04E05 phosphors excited at 348 nm excitation

phosphors. The CCT values for the visible emission for $Ba_{2-x}Dy_{0.04}Eu_xV_2O_7$ phosphors were obtained using McCamy's empirical (Eq. (8)): [65, 66] methodology:

$$CCT = -499n^3 + 3525n^2 - 6823n + 5520.33 \tag{8}$$

It was proved that when the as-synthesized phosphors were excited at 305 nm, the bluish-white color emission was exhibited for BD04E01, BD04E02, BD04E03, BD04E04, and BD04E05 phosphors. Figure 7 shows the as-prepared $Ba_{2-x}Dy_{0.04}Eu_xV_2O_7$ phosphors when excited under 348 nm, and the emission color was tuned from bluish-white to greenish-yellow region. The CRI and CCT values were changed when the Eu^{3+} concentration was increased. From the summary results provided in Table 2, it is determined that the as-prepared $Ba_{2-x}Dy_{0.04}Eu_xV_2O_7$ phosphors can be used for the UV and near-UV phosphor-converted WLEDs (Table 2).

4. Conclusions

A series of single-phase $Ba_{2-x}Dy_{0.04}Eu_xV_2O_7$ phosphors ($x = 0.01, 0.02, 0.03, 0.04,$ and 0.05) were synthesized by hydrothermal method. The powder XRD patterns for BD04E01, BD04E02, BD04E03, BD04E04, and BD04E05 phosphors confirm that the dopant is substituted on the host lattice without changing its crystal system. A meta-stable state between the valence and conduction bands is confirmed by diffused reflectance spectra caused by Eu^{3+} substitution in the prepared $Ba_{2-x}Dy_{0.04}Eu_xV_2O_7$ phosphors. The photoluminescence spectra further confirm the doping of the Eu^{3+} ion. The PL spectra recorded at 348 nm tunes emission color from bluish-white to greenish-yellow.

Fig. 8 Images of BD04E01, BD04E02, BD04E03, BD04E04, and BD04E05 phosphors excited by 365 nm under a UV lamp and their corresponding day light images
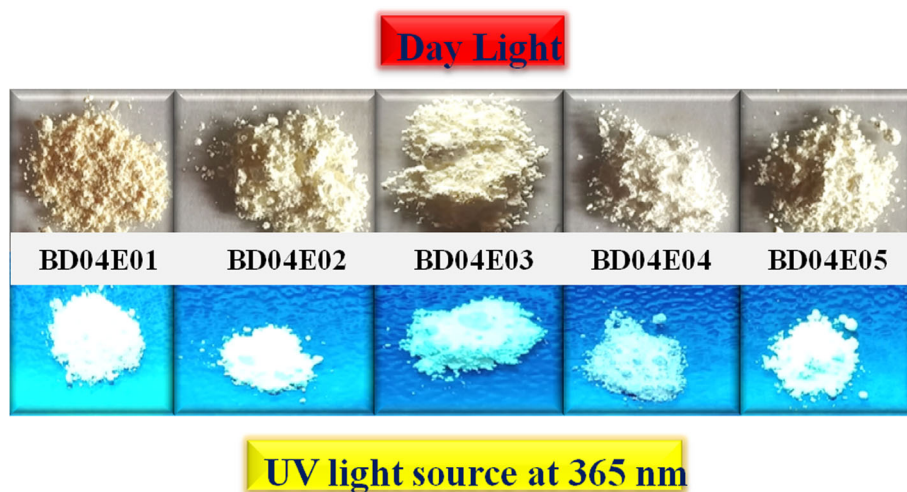

Table 2 Comparison of CIE coordinates and CCT of BD04E01, BD04E02, BD04E03, BD04E04, and BD04E05 phosphors under 348 nm excitation

Excitation wavelength	Eu^{3+} concentrations (x)	CIE coordinates (x, y)	CCT (K)
	0.01%	(0.2319,0.3494)	6318
	0.02%	(0.2196,0.3220)	6245
348 nm	0.03%	(0.3580,0.5131)	6925
	0.04%	(0.3547,0.5069)	6906
	0.05%	(0.3544,0.5216)	6922

The white color emission of $Ba_{2-x}Dy_{0.04}Eu_xV_2O_7$ phosphors is verified and confirmed by the irradiation under the UV light 365 nm for WLED applications. In summary, it is concluded that the Dy^{3+}/Eu^{3+}-co-doped $Ba_{2-x}Dy_{0.04}Eu_xV_2O_7$ phosphors have the potential ability for application in UV and near-UV phosphor-converted WLEDs.

Declarations

Conflict of interest The authors declare and claim no conflicts of interest.

References

[1] J C G Bunzli and C Piguet *Chem. Soc. Rev.* **34** 1048 (2005).

[2] Z Wei, H Ping, T Datao and M En *Soc. Rev.* **44** 1379 (2015).

[3] K Taeho et al. *RSC Adv.* **4** 45687 (2014).

[4] X Chen, Y Liu and D Tu *Springer-Verlag Berlin Heidelberg* 75 (2014)

[5] L Yongsheng, T Datao, Z Haomiao and C Xueyuan *Chem. Soc. Rev.* **42** 6924 (2013).

[6] G Shili and L Chunxia *Rev.* **114** 2343 (2014).

[7] P Jin Young, C Jong Won and Y Hyun Kyoung *Optik.* **155** 384 (2018).

[8] F Hongwei, W Xiantao, Z Shaoshuai and C Yonghu *Chem.* **55** 9284 (2016).

[9] M Xiaoyun, D Kai, H Kai, Z Peng, G Dongling and Z Yang *Res. Bull.* **60** 72 (2014).

[10] R Urlagaddala, M Nagegownivari Ramachandra, R Busireddy Sudhakar and C Sandip *Lumin.* **31** 141 (2016).

[11] D Mandeep, V B Taxak and C Sangeeta *J. Phy. Chem. Solids* **89** 45 (2016).

[12] C Xue, X Zhiguo and Y Min *J. Phys. Chem. Solids* **74** 1439 (2013).

[13] H Kim and J Kim *J. Nanosci. Nanotechnol.* **16** 1827 (2016).

[14] E Pavitra *Rep.* **5** 10296 (2015).

[15] Z Wentao, C Li and Z Dongshengv *J. Ceram. Int.* **44** 5420 (2018).

[16] E F Kewele and F D Birhanu *Matt.* **535** 245 (2018).

[17] Z-P Ci *Phys. B.* **19** 057803 (2010).

[18] S Neeraj *State. Comm.* **131** 65 (2004).

[19] L Bo and S Chaoshu *J. Alloys. Compd.* **333** 215 (2002).

[20] M Manoj Kumar, K Kaushal and K R Vineet *Senor. Act B: Chem.* **209** 775 (2015).

[21] Z Yuhui, H Jing and D Surong *J. Elect. Mater.* **45** 2974 (2016).

[22] T Qinxue, Q Kehui, L Junfeng, Z Wentao and Z Yu *J. Mater. Sci: Mater. Electron.* **28** 18686 (2017).

[23] L Kai and D Rik Van *Dyes Pigment.* **155** 258 (2018).

[24] Z Xinguo, Z Zhenpeng and S Zishan *J. Lumin.* **203** 735 (2018).

[25] N Venkatesh Bharathi, T Jeyakumaran, S Ramaswamy and S S Jayabalakrishnan *Mater. Res. Express.* **6** 106202 (2019).

[26] Z Jiangcong, H Xiaotian, Y Jinhui and W Bo *J. Ceram. Int.* **45** 13832 (2019).

[27] Z Jiangcong, Y Yao, C Yu, W Bo, H Xiaotian and L Yiqing *J. Ceram. Int.* **46** 6276 (2020).

[28] H Sk Khaja, G Tran Thi Hoai and Y Jae Su *J. Alloys. Compd.* **739** 218 (2018).

[29] C Hande and Z Jiangcong *Mater.* **89** 132 (2019).

[30] M Mingyue, L Haidong, C Fengmei and P Daocheng *Thin Solid Films* **676** 133 (2019).

[31] T Liv, C Shan-min, L Qiang, W Jie-ling and Z Rui-ni *Nonferr. Met. Soci. China* **30** 1031 (2020).

[32] C Min, Q Kehui and Z Peicong *J. Ceram. Int.* **45** 22547 (2019).

[33] H Wentao, L Quan, L Xibing, Z Qingwen, W Lixi and Z Qitu *J. Ceram. Int.* **45** 15624 (2019).

[34] Y Lixin, M Xiaoyun, Z Huiling and Z Xiyan *J. Alloys. Compd.* **787** 815 (2019).

[35] P Harishkumarreddy, H S K Khaja, L Krishna Bharat and Y Jae Su *Dyes and Pigments.* **162** 583 (2019).

[36] W Yuexin, S Yanhua, Z Xiuqing, L Yi, C Tingting and Z Keyan *Eng. J.* **306** 155 (2016).

[37] M K Anna, N Dorine and D Rik Van *Dalton Trans RSC* **45** 16231 (2016).

[38] Z Xuemei, T Qinyue, H Shanshan and Y Jun *Mater. Chem. Phys.* **215** 259 (2018).

[39] W Xiulan, B Wenni, H Ou and R Qiang *J. Solid. State. Chem.* **265** 109 (2018).

[40] P Mingying and P Zhiwu *J. Mater. Chem.* **13** 1202 (2003).

[41] L Simei, D Bin, C Jun, L Hui, Z Chong-song and Y Ruijin *IOP Conf. Ser.: Earth Environ. Sci.* **295** 032035 (2019).

[42] R Rajesh Kanna et al. *Inter.* **46** 13695 (2020).

[43] T Mami, H Manabu and F Shinobu *Inorg. Chem.* **55** 7879 (2016).

[44] L Shiqi, L Yujun, Z Yingli, L Haoran and C Jiahui *J. Amer. Ceram. Soci.* **101** 1655 (2018).

[45] T Jeyakumaran *J. Inorg. Organomet. Polym.* **31** 674 (2021).

[46] K Vinod, P Anurag and O M Ntwaeaborwa *J. Alloys. Compd.* **708** 922 (2017).

[47] M S Sajna, G Subash, V P Prakashan, M S Sanu and J Cyriac *Mater.* **70** 31 (2017).

[48] J Zhou, F Huang and J Xu *J. Mater. Chem. C* **3** 3023 (2015).

[49] R Cao, D Peng, H Xu, Z Luo, H Ao, S Guo and J Fu *Optik.* **127** 7896 (2016).

[50] P Kumari and J Manam *RSC Adv.* **5** 107575 (2015).

[51] P Niu and X Liu *J. Mater. Sci: Mater. Electron.* **29** 124 (2018).

[52] Q Tang, K Qiu, J Li, W Zhang and Y Zeng *J. Mater. Sci.: Mater. Electron.* **28** 18686 (2017).

[53] K Astha *Acta Part A* **127** 98 (2014).

[54] E Pavitra, G S R Raju, L K Bharat, J Y Park, C H Kwak and J W Chung *J. Mater. Chem. C* **6** 12746 (2018).

[55] L Kai and D Rik Van *ACS Sustainable. Chem. Eng.* **7** 16284 (2019).

[56] L Kai and D Rik Van *ACS Appl. Electron. Mater.* **2** 1735 (2020).

[57] B Koen *Coord. Chem. Rev.* **295** 1 (2015).

[58] A R Dhobale and M Mohapatra *J. Lumin.* **132** 293 (2012).

[59] J J Dragana, C Andrea, Z Lidia and V G Tamara *Mater.* **76** 308 (2018).

[60] G Dongling, L Guogang, S Mengmeng, P Chong, Z Yang, C Ziyong and L Jun *Dalton Trans.* **41** 3078 (2012).

[61] P Sasank and R Vineet *Mater. Res. Bull.* **125** 110761 (2020).

[62] L Jun, D Huawei and Z Yueli *Chem. Chem. Phy.* **17** 15412 (2015).

[63] X Wu, W Bai, O Hai, Q Ren, F Lin and Y J Jiao *Solid State Chem.* **265** 109 (2018).

[64] K N Shinde *J. Lumin.* **145** 588 (2014).

[65] C Haochiang, H Yu Lin and Y Chu *J. Am. Ceram. Soc.* **97** 3737 (2014).

[66] W Zhang, H Shen, X Hu, Y Wang, J Li and Z Zhu *J. Alloys. Compd.* **781** 255 (2019).